Conformational Specificity of the *Lac* Repressor Coiled-Coil Tetramerization Domain[†,‡]

Jie Liu,[§] Qi Zheng,[§] Yiqun Deng,[§] Qunnu Li,[§] Neville R. Kallenbach,[||] and Min Lu*[,§]

Department of Biochemistry, Weill Medical College of Cornell University, New York, New York 10021, and Department of Chemistry, New York University, New York, New York 10003

Received September 21, 2007

ABSTRACT: Predictive understanding of how the folded, functional shape of a native protein is encoded in the linear sequence of its amino acid residues remains an unsolved challenge in modern structural biology. Antiparallel four-stranded coiled coils are relatively simple protein structures that embody a heptad sequence repeat and rich diversity for tertiary packing of α-helices. To explore specific sequence determinants of the *lac* repressor coiled-coil tetramerization domain, we have engineered a set of buried nonpolar side chains at the *a*-, *d*-, and *e*-positions into the hydrophobic interior of the dimeric GCN4 leucine zipper. Circular dichroism and equilibrium ultracentrifugation studies show that this core variant (GCN4-pAe$_{LV}$) forms a stable tetrameric structure with a reversible and highly cooperative thermal unfolding transition. The X-ray crystal structure at 1.9 Å reveals that GCN4-pAe$_{LV}$ is an antiparallel four-stranded coiled coil of the *lac* repressor type in which the *a*, *d*, and *e* side chains associate by means of combined knobs-against-knobs and knobs-into-holes packing with a characteristic interhelical offset of 0.25 heptad. Comparison of the side chain shape and packing in the antiparallel tetramers shows that the burial of alanine residues at the *e* positions between the neighboring helices of GCN4-pAe$_{LV}$ dictates both the antiparallel orientation and helix offset. This study fills in a gap in our knowledge of the determinants of structural specificity in antiparallel coiled coils and improves our understanding of how specific side chain packing forms the teritiary structure of a functional protein.

The *lac* repressor interacts with its cognate operator sequence to form a genetic switch that coordinately regulates transcription of the *lac* operon and thus controls lactose utilization in *Escherichia coli* (*1*). The quaternary structure of the repressor comprises four N-terminal headpieces that bind to operator DNA and a C-terminal tetrameric core that binds inducer (*1*, *2*). Tetramerization of the core domain is mediated by a 19-residue sequence (*3*, *4*) that contains an unusual 7-amino acid repeat with aliphatic side chains at the first (*a*), fourth (*d*), and fifth (*e*) positions (called a 3−3−1 hydrophobic repeat, in accord with the well-known convention for coiled coils) (*5*). Genetic analysis has revealed that this heptad repeat at the extreme C terminus of the protein can associate to form a tetramer of α-helices in an antiparallel relative orientation (*6*) and that uncharged amino acids at the *e* positions play an essential role in specifying this tetramolecular structure (*6*). Mutations and deletions in the C terminus of the *lac* repressor abolish tetramer formation and reduce inducer binding activity (*7*−*9*). Furthermore, peptide models of the heptad-repeat region fold into stable, antiparallel four-helix bundles in solution (*10*, *11*). The crystal structure of the *lac* repressor shows that buried *a*, *d*, and *e* residues in the region of contact between the four α-helices form atypical interlocking hydrophobic seams (*12*, *13*). These coiled-coil interactions contribute to stabilizing the *lac* repressor tetramer that regulates cooperativity of ligand binding.

The α-helical coiled coil is among the most common protein motifs found in nature and has proven to be a fundamental model system for investigating the interplay between the amino acid sequence and structure of α-helical protomers (*14*−*20*). The conformation of a classical coiled coil is prescribed by the 3−4 hydrophobic heptad repeat, with apolar amino acids spaced every four and then every three residues (*21*−*24*). The hydrophobic residues occur at positions *a* and *d* of the heptad repeat, whereas residues at positions *e* and *g* are predominantly charged. The interacting surface between supercoiled helices is formed by Crick's knobs-into-holes meshing of the nonpolar *a* and *d* side chains (*25*, *26*). In fact, stereochemical features of this surface have been shown to impart oligomerization and orientation specificity (*26*−*31*). Polar side chains at the *a* and *d* positions also can destabilize coiled-coil structure yet impart partner specificity and helix-orientation preference (*32*−*35*). Moreover, electrostatic interactions between oppositely charged residues at the *e* and *g* positions of different strands are implicated in regulating structural selectivity, although their relative contributions to stabilizing a target conformation versus destabilizing alternative states have been difficult to untangle (*36*−*43*). These coiled-coil interactions a priori are expected to be applicable to both parallel and antiparallel

[†] This work was supported by NIH Grant AI68591 and by the Irma T. Hirschl Trust.

[‡] The atomic coordinates and structure factors have been deposited in the RCSB Protein Data Bank (entry 2R2V).

* To whom correspondence should be addressed. Phone: (212) 746-6562. Fax: (212) 746-8875. E-mail: mlu@med.cornell.edu.

[§] Weill Medical College of Cornell University.

[||] New York University.

10.1021/bi701930d CCC: $37.00
Published on Web 12/04/2007

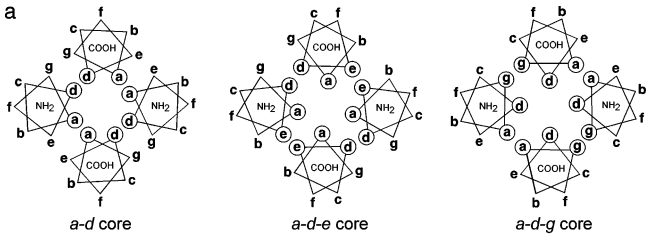

FIGURE 1: Core packing in antiparallel four-stranded coiled coils. (a) Helical wheel representation of the D_2-symmetric tetramer showing interhelix contacts at positions *a* and *d* (*a*−*d* core), *a*, *d*, and *e* (*a*−*d*−*e* core), and *a*, *d*, and *g* (*a*−*d*−*g* core). Heptad-repeat positions are labeled *a*−*g*. The N and C termini of the helices are indicated. (b) Amino acid sequence of the GCN4-pAe$_{LV}$ peptide described in this study. GCN4-pAe$_{LV}$ differs from the recombinant dimeric leucine-zipper peptide GCN4-pR only by the amino acids present at positions *a*, *d*, and *e*.

structures. However, optimal interaction of the core *a* and *d* residues in the antiparallel configuration requires an axial stagger of the heptad repeat, rather than side by side as in the parallel case. As a consequence of this geometrical requirement, the paired antiparallel helices are associated with a relative axial translation (*44*), while the helical offset is close to zero in classical parallel coiled coils. Parallel and antiparallel coiled coils also have different interactions on the surface, with *g* to *e*′ interactions in parallel structures versus *e* to *e*′ and *g* to *g*′ in antiparallel structures.

In practice determinants of parallel structure are embodied in the development of sequence-based algorithms for recognizing coiled-coil motifs in the human genome (*22*, *23*, *45*−*51*). Attempts to combine computational design and experimental characterization to understand the specificity of coiled-coil protein interactions at a high level of detail have begun (*52*, *53*). In contrast, the determination of antiparallel coiled-coil assembly of α-helices is less well-understood, in part because structurally characterized, naturally occurring antiparallel coiled coils are frequently short and intramolecular, limiting the information available for these systems (*14*). Some structural determinants of antiparallel coiled coils have been characterized in model peptide constructs, as noted above. Although antiparallel coiled coils have been successfully designed by exploiting these general principles (*38*, *43*, *54*, *55*), helix orientation cannot be accurately predicted from the amino acid sequence in most coiled coils. The presence of apolar amino acids at either the *e* or *g* position in the heptad repeat can direct formation of stable, antiparallel four-stranded coiled coils (see Figure 1a) (*10*, *11*, *42*, *56*, *57*). The helices of these tetramers associate via nonclassical knobs-into-holes packing interactions, and the backbones of neighboring strands are staggered to ensure a good mechanical fit (*42*, *44*). The *lac* repressor type of core packing, for example, is of the *a*, *d*, *e* class, with the helices shifted by half a turn of the two-turn repeat (measured as the distance between planes orthogonal to the helix axes centered at the C$^{\alpha}$ atoms of the *a* positions of the proximal helices) (*10*, *13*). On the other hand, in the GCN4-pV peptide, the packing involves the *a*, *d*, and *g* side chains with a helix offset of one full turn (*42*). In this connection, the Richardson's distinguished two types of tightly packed, antiparallel helix arrangements they referred to as "Alacoils" (*44*), in which the backbones of two associating helices are offset either by half a turn with alanine in position *e* (the ferritin type) or by a full turn with alanine at position *g* (the Rop type). Thus, heptad shifts in register are important structural features of antiparallel tetramer configurations (*10*, *11*, *42*). Because coiled coils have proven valuable for understanding how interfacial interactions between proteins are encoded in their sequences, detailed studies of sequence−structure relationships in the antiparallel tetramers have broad implications for our understanding of protein structure, folding, and design.

The goal of our present study is to identify specific sequence determinants of the coiled-coil interfaces in the *lac* repressor tetramerization domain and to understand the basis of structural specificity in antiparallel four-stranded coiled coils. We demonstrate that buried nonpolar side chains at the *a*, *d*, and *e* positions of the heptad repeat specify and stabilize the *lac* repressor type of antiparallel tetramer conformation in a background of the GCN4 leucine zipper sequence. The requirement to accommodate small alanine residues at the *e* positions dictates the interior packing and helix register in the engineered leucine-zipper tetramer. We also attempt to define structural principles underlying the conformation and topology in antiparallel tetrameric coiled coils. A comprehensive understanding of such principles will allow formulation of fundamental rules for coiled-coil protein prediction and design and can be used to design new protein−protein interfaces with specific biological functions.

MATERIALS AND METHODS

Cloning and Protein Production. Recombinant DNA procedures were carried out by standard methods, and all generated sequences were confirmed by DNA sequencing. A synthetic gene encoding GCN4-pAe$_{LV}$ (see Figure 1b) was prepared with optimal codon usage for *E. coli* and subsequently cloned into the *Nde*I−*Bam*HI sites of a modified pET3a vector (Novagen, San Diego, CA). The GCN4-pAe$_{LV}$ peptide was expressed in the *E. coli* strain BL21(DE3)/pLysS (Novagen, San Diego, CA). Cells were grown at 37 °C in Luria−Bertani (LB)[1] medium to an optical density of 0.7 at 600 nm and induced with isopropyl thio-*β*-D-galactoside (IPTG) for 3 h at 37 °C. The cells were lysed by addition of glacial acetic acid and clarified by centrifugation at 35000*g* for 30 min. The soluble fraction containing peptide was subsequently dialyzed into 5% (v/v) acetic acid overnight at 4 °C. The peptide was purified to homogeneity by reverse-phase HPLC (Waters, Inc.) on a C18 preparative column (Hesperia, CA) using a water−acetonitrile gradient in the presence of 0.1% (v/v) trifluoroacetic acid. Peptide identities were confirmed by electrospray mass spectrometry (Voyager Elite, PerSeptive Biosystems, Framingham, MA). Protein concentrations were determined by tyrosine absorbance at 280 nm in 6 M GuHCl (*58*).

Circular Dichroism (CD) Spectroscopy. CD experiments were performed on an Aviv 62A/DS (Aviv Associates, Lakewood, NJ) spectropolarimeter equipped with a thermo-

[1] Abbreviations: LB, Luria−Bertani; IPTG, isopropyl thio-*β*-D-galactoside; HPLC, high-performance liquid chromatography; CD, circular dichroism; TBS, Tris-buffered saline; GuHCl, guanidine hydrochloride; $[\theta]_{222}$, molar ellipticity at 222 nm; T_m, midpoint of the thermal unfolding transition; rms, root mean square.

electric temperature controller in TBS (50 mM Tris−HCl, pH 8.0, 150 mM NaCl). CD spectra were collected from 260 to 200 nm at a 50 μM peptide concentration, using an average time of 5 s, a cell path length of 0.1 cm, and a bandwidth of 1 nm. A $[\theta]_{222}$ value of −33 000 deg cm^2 dmol^{-1} was taken to correspond to 100% helix (*59*). Thermal stability was determined in the same buffer at 5 μM peptide concentration by monitoring $[\theta]_{222}$ as a function of temperature with a 1 cm path length cell. Thermal melts were performed in 2 deg intervals with a 2 min equilibration at the desired temperature and an integration time of 30 s. Reversibility was checked by repeated scans. All melts were reversible, with superimposable folding and unfolding curves, and >95% of the signal regained upon cooling. The midpoint of the cooperative thermal unfolding transition (T_m) was determined from $[\theta]_{222}$ versus temperature data by evaluating the maximum of $d[\theta]/dT^{-1}$ (*60*).

Sedimentation Equilibrium Analysis. Analytical ultracentrifugation measurements were made on a Beckman XL-A analytical ultracentrifuge (Beckman Coulter, Fullerton, CA) equipped with an An-60 Ti rotor at 20 °C as described (*61*). Peptide solutions were dialyzed overnight against TBS (pH 8.0), loaded at initial concentrations of 20, 150, and 1000 μM, and analyzed at rotor speeds of 25 and 28 krpm. Data were acquired at two wavelengths per rotor speed setting and processed simultaneously with a nonlinear least-squares fitting routine (*62*). The solvent density and protein partial specific volume were calculated according to the solvent and protein composition, respectively (*63*). Random residuals were observed in all cases.

Crystallization and Structure Determination. GCN4-pAe$_{LV}$ was crystallized at room temperature using the hanging drop vapor diffusion method by equilibrating against reservoir buffer (100 mM sodium citrate (pH 4.8), 5% (v/v) Jeffamine M-600, 50 mM zinc acetate), a solution containing 1 μL of 15 mg/mL peptide in water, and 1 μL of reservoir buffer. The crystals belong to space group $P4_3$ ($a = b = 51.70$ Å, $c = 99.79$ Å) and contain eight monomers in the asymmetric unit. The crystals were transferred into cryosolution containing the reservoir buffer and 30% (v/v) glycerol, harvested, and frozen in liquid nitrogen. Diffraction data were collected on beamline X4A at the National Synchrotron Light Source (Brookhaven, NY). Reflection intensities were integrated and scaled with DENZO and SCALEPACK (*64*). Initial phases were determined by molecular replacement with Phaser (*65*) using the structure of the GCN4-pAe monomer (*66*) as a search model. Eight GCN4-pAe molecules were oriented and placed in the asymmetric unit, corresponding to the eight GCN4-pAe$_{LV}$ chains. This model and the dataset for GCN4-pAe$_{LV}$ were directly fed to Arp/Warp (*67*), which provided a largely complete asymmetric unit of the eight chains and allowed ∼90% of the final model to be interpreted. The resulting electron density map was of excellent quality and showed the location of most of the side chains. Crystallographic refinement of the GCN4-pAe$_{LV}$ structure was carried out using Refmac (*68*). Density interpretation and manual model building were done with O (*69*). The final model ($R_{cryst} = 19.1\%$ and $R_{free} = 24.0\%$ for the resolution range 51.7−1.90 Å) consists of residues 2−34 (monomer A), 1−33 (monomer B), 1−33 (monomer C), 2−34 (monomer D), 1−31 (monomer E), 3−34 (monomer F), 1−33 (monomer G), and 3−33 (monomer H) in the asymmetric unit and 99 water molecules. The bond lengths and bond angles of the model have root-mean-square (rms) deviations from ideality of 0.009 Å and 1.1°, respectively. All residues but two (Lys-B2 and Lys-G2) occupy the most preferred regions of the Ramanchandran plot. Lys-B2 and Lys-G2 lie in allowed regions of the Ramanchandran space and are the second residue from the N terminus.

Structure Analysis. Coiled-coil parameters were calculated by using TWISTER (*70*). The rms deviations were calculated with LSQKAB in the CCP4i program suite (*71*). Buried surface areas were calculated from the difference of the accessible side chain surface areas of the tetramer and of the individual helical monomers using CNS 1.0 (*72*). Figures were generated using SETOR (*73*), MOLSCRIPT (*74*), and Raster 3D (*75*).

RESULTS AND DISCUSSION

Engineering the Lac Repressor Type of Antiparallel Tetramer. In the *lac* repressor coiled-coil tetramerization domain, bulky aliphatic amino acids at the central *a* positions form hydrophobic seams linking four antiparallel helices, resulting in the recruitment of peripheral interactions at the flanking *d* and *e* positions to sequester the interfacial *a* position residues from solvent (Figure 1a) (*1*, *2*, *10*, *11*). The orientation and oligomerization state of this antiparallel tetramer cannot be predicted from the amino acid sequence, and the determinants of its structural specificity cannot easily be explained using known general principles. The *lac* repressor coiled-coil structure apparently conforms to the ferritin type of Alacoil, that is, to an interhelical offset of half a turn (*11*). Its heptad-repeat sequence reveals alanine predominantly at the *e* positions, consistent with the need for the methyl groups to favor an antiparallel association of helices (*11*, *44*, *76*, *77*). However, simple inclusion of alanine at the *e* position of the heptad repeat is insufficient to determine the *lac* repressor pattern of the core packing arrangement (*78*). Because protein engineering has proven to be a powerful tool for understanding protein folding and function, we decided to probe, at atomic resolution, specific sequence determinants of the *lac* repressor coiled-coil fold by mutating residues at the *a*, *d*, and *e* positions of the prototypical homodimeric GCN4 leucine zipper. The hydrophobic interface between the two *a*-helical chains of the leucine zipper is formed by interspersing nonpolar side chains at the *a* and *d* positions with hydrophilic residues at the flanking *e* and *g* positions (*79*). In attempting to reconstruct the *lac* repressor type of coiled-coil interfaces, we engineered a recombinant leucine-zipper GCN4-pR variant called GCN4-pAe$_{LV}$ that contains five leucines at the *a* positions, three valines and one asparagine at the *d* positions, and four alanines at the *e* positions (Figure 1b). Asn17 at the third *a* heptad position of the parent GCN4-pR molecule was retained to occupy the same heptad *d* position in GCN4-pAe$_{LV}$.

GCN4-pAe$_{LV}$ Forms a Stable α*-Helical Tetramer in Solution*. The bacterially expressed GCN4-pAe$_{LV}$ peptide exhibits a characteristic α-helical CD spectrum with negative minima at ∼222 and ∼209 nm in physiological aqueous solution (Figure 2a). The mean residue ellipticity of the folded peptide at 222 nm is −32 600 deg cm^2 dmol^{-1}, consistent with an essentially 100% helical structure (*59*).

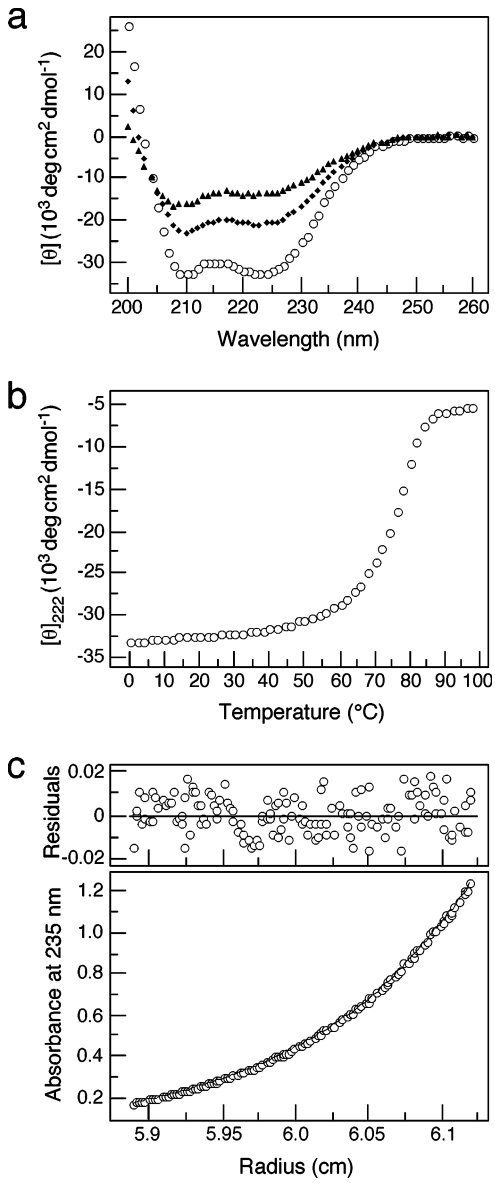

FIGURE 2: GCN4-pAe$_{LV}$ associates to form a very stable tetramer of α-helices. (a) Circular dichroism spectra at 0 °C (circles), 80 °C (tilted squares), and 90 °C (triangles) in TBS (pH 8.0) and 50 μM peptide concentration. (b) Thermal dependence of the circular dichroism signal at 222 nm in 5 μM peptide concentration. (c) Representative sedimentation equilibrium data at 20 °C and 28 krpm in TBS (pH 8.0) and 150 μM peptide concentration. The data fit closely to a tetrameric complex. The deviation in the data from the linear fit for a tetrameic model is plotted (upper).

GCN4-pAe$_{LV}$ undergoes a cooperative and reversible thermal unfolding transition (Figure 2b). The midpoint of the temperature dependence (T_m) of the ellipticity at 222 nm is 75 °C at a peptide concentration of 5 μM. The progressive increase of this T_m value with increasing peptide concentration suggests that GCN4-pAe$_{LV}$ self-associates. Equilibrium ultracentrifugation experiments indicate that the GCN4-pAe$_{LV}$ peptide sediments as a discrete tetramer; its apparent molecular mass is 15.3 kDa in the concentration range of 20 μM to 1 mM (Figure 3c). We conclude that the concentration dependence of the T_m for GCN4-pAe$_{LV}$ reflects a monomer-to-tetramer equilibrium and that the folded tetramer is well-ordered and very stable. Therefore, the extended core residues at the *a*, *d*, and *e* positions of GCN4-pAe$_{LV}$ are responsible for mediating homotetramer formation.

Three-Dimensional Structure. To evaluate the structural features of the *a*, *d*, *e* core packing of the tetramer in atomic detail, we determined the X-ray crystal structure of the GCN4-pAe$_{LV}$ peptide at 1.9 Å resolution (Table 1). The engineered peptide forms the intended antiparallel, four-stranded coiled-coil structure (Figure 3). This left-handed supercoil comprises a cyclinder ~50 Å in length and ~25 Å in diameter. Diagonally related helices have identical relative orientation and are aligned without lateral displacement (Figure 3b). The backbones of adjacent antiparallel helices are shifted from each other by half a turn. The crossing angle between neighboring helices is near 23°. Individual helices in the tetramer can be superimposed on each other with an rmsd for C$^{\alpha}$ atoms of 0.17−0.80 Å. The distance between the axes of parallel helices (on diagonal) is ~14 Å, whereas that between the axes of adjacent antiparallel helices is ~8−11 Å (Table 2). The antiparallel tetramer has approximate D_2 symmetry with a 2-fold axis coincident with the superhelical axis, as well as two orthogonal 2-fold axes directed between the helices. Therefore, GCN4-pAe$_{LV}$ assumes the overall antiparallel coiled-coil configuration of the *lac* repressor tetramerization domain.

The leucine side chains at the *a* positions interact between parallel helices and stagger axially to form the tetramer interface (Figure 3a), which consists of 10 hydrophobic layers. Each cross-sectional *a* layer contains two leucine residues (Figure 3c), which alternate from one pair of parallel helices to the other. Eighteen of the 20 leucine side chains adopt χ_1 and χ_2 dihedral angles near −65°, 175° or −177°, 65°, corresponding to their most favored rotamers in α-helices (*80*). Residues at the *d* and *e* positions of the neighboring antiparallel helices pack against the leucines at *a* to complete the hydrophobic core (Figure 3d). Relative to the side chains of isolated helices, the leucine side chains at the *a* positions of the tetramer are completely buried, residues at the *d* and *e* positions are substantially buried (~94%), those at the *b* and *g* positions are partly buried (29 and 45%, respectively), and the *c* and *f* positions remain completely exposed. Approximately 5830 Å^2 of solvent-accessible surface area (44% of the total accessible surface area of the four helical monomers) is buried in the tetramer.

The tetramer shows "knobs-against-knobs" packing of the leucine side chains at the central *a* positions between aligned, parallel helices (Figure 3b,c). The C$^{\alpha}$−C$^{\beta}$ bonds of leucine knobs incline by ~45° toward the N terminus of each helix with respect to the plane perpendicular to the superhelical axis. This geometry maximizes hydrophobic interactions between the side chains. The tetramer also makes peripheral "knobs-into-holes" contacts between shifted, adjacent antiparallel helices. Leucine knobs at the *a* positions fit into triangles formed by the *d* and *e* residues of the other helix and by an adjacent *a* leucine layer of the preceding heptad. Knobs formed by *d* residues fit into triangles formed by the *a* and *g* residues of the other helix and by an adjacent *d* residue layer of the preceding heptad. Similarly, alanine knobs at the *e* positions pack into triangles formed by the *a* and *b* residues of the other helix and by an adjacent *e* alanine layer. Thus, the *a*, *d*, and *e* residues of the heptad repeat segregate into four distinct types of helix contacts to create alternating rectangular cross-sections. In summary, these conjoined core and peripheral packing interactions specify the unique antiparallel tetramer structure that is the energeti-

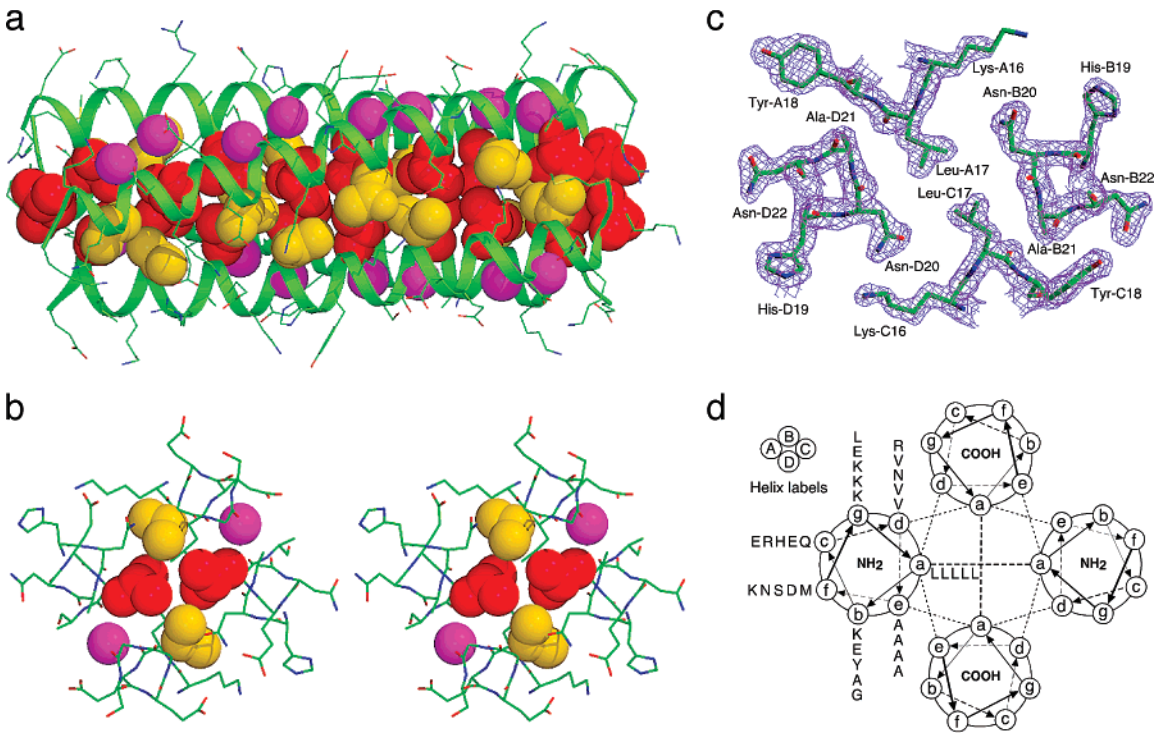

FIGURE 3: Crystal structure of the GCN4-pAe$_{LV}$ tetramer. (a) Lateral view of the antiparallel tetramer. Red van der Waals surfaces identify leucine residues at the *a* positions, yellow surfaces identify residues at the *d* positions, and magenta surfaces identify alanine residues at the *e* positions. (b) Stereoview of antiparallel packing in the tetramer. The van der Waals surfaces are colored red for Leu-A24 (*a*) and Leu-C24 (*a*), yellow for Val-B13 (*d*) and Val-D13 (*d*), and magenta for Ala-B14 (*e*) and Ala-D14 (*e*). (*c*) Representative $2F_o - F_c$ electron density map (contoured at 1.5σ). (d) Helical wheel representation of the tetramer. Heptad positions are labeled *a*−*g*.

Table 1: Crystallographic Data and Refinement Statistics

Data Collection	
temp (K)	100
X-ray source	NSLS X4A
space group	$P4_3$
cell dimensions (Å)	$a = b = 51.70$, $c = 99.79$
no. of molecules in the AU	8
solvent content (%)	44
resolution (Å)	51.7−1.90
no. of total reflns	432 508
no. of unique reflns	20 545
multiplicity	5.0
completeness (%)	99.7 (99.9)[a]
no. of reflns $>2\sigma_I$	17 496
$I/\sigma(I)$	13.2
R_{merge}[b] (%)	6.1
Refinement	
resolution (Å)	51.7−1.90
no. of protein atoms	2 045
no. of water molecules	99
no. of zinc ions	2
no. of citrate ions	4
no. of acetate ions	3
R_{cryst}/R_{free}[c] (%)	19.1/24.0
rmsd bond lengths (Å)	0.009
rmsd bond angles (deg)	1.1
rmsd torsion angles (deg)	4.3
av *B* factors (Å^2)	37.5
estimated error for *B* factors (Å^2)	6.0

[a] Values in parentheses refer to the highest resolution shell, 1.97−1.90 Å. AU = asymmetric unit. [b] $R_{merge} = \sum|I - \langle I\rangle|/\sum I$, where I is the integrated intensity of a given reflection. [c] $R_{cryst} = \sum|F_o - F_c|/\sum F_o$. $R_{free} = R_{cryst}$ calculated by using 5% of the reflection data chosen randomly and omitted from the start of refinement.

cally most favorable state. The results support the proposal that the amino acid sequence at the buried *a*, *d*, and *e* positions is an essential determinant of the *lac* repressor coiled-coil tetramer fold (*6*, *10*, *11*).

Principles of Packing in Antiparallel Tetrameric Coiled Coils. There are at least five types of antiparallel helix packing arrangements in structurally characterized antiparallel four-stranded coiled coils (Figure 4): the well-known *a*−*d* pattern with ∼0.5 heptad offset (Rop), an *a*−*d* pattern with ∼0.25 heptad (WSPLB and E20C), an *a*−*d*−*e* triad with ∼0.25 heptad (*lac* repressor and GCN4-pAe$_{LV}$), an *a*−*d*−*g* triad with ∼0.25 heptad (SARS C44 and GCN4-pA), and an *a*−*d*−*g* triad with ∼0.5 heptad (GCN4-pV) (Table 2). Although the superhelical pitch, radius, residues per turn, and interhelix separation differ significantly in these coiled-coil structures, the individual α-helices are virtually identical on a local scale, and adjacent antiparallel helices have similar cross-angles to allow for knobs-into-holes core packing. Comparison of side chain shape and packing in the antiparallel tetramers suggests that the requirement to satisfy the complementary packing potential of buried hydrophobic residues is the basis of configurational specificity.

In the Rop tetramer, the vertical translation of approximately 0.5 heptad results in a displacement equal to one helical turn and thus leads to an approximate layering of *a*−*d* pairs between aligned helix backbones (Figure 4b). Each core packing layer consists of two large and two small *a* and *d* residues with an 8.6 Å by 10.0 Å rectangular cross-section (for example, Leu-A22 (*d*), Cys-A38 (*a*), Ala-B12 (*a*), and Leu-B48 (*d*); Figure 4a) (*31*, *81*). By contrast, in the E20C tetramer adjacent helices are offset by half a turn such that the *a* layers containing two leucines alternate with the *d* layers containing two isoleucines (Figure 4c,d). This geometry results in a knobs-into-holes packing of these large residues by compensating for the altered $C^{\alpha}-C^{\beta}$ vectors due

Table 2: Superhelical Characteristics of Antiparallel Four-Stranded Coiled Coils[a]

parameter	Rop	WSPLB	E20C	*lac*	GCN4-pAe$_{LV}$	GCN4-pA	C44	GCN4-pV
core packing pattern	a−d	a−d	a−d	a−d−e	a−d−e	a−d−g	a−d−g	a−d−g
fraction offset (heptad)	0.43	0.19	0.28	0.26	0.26	0.31	0.26	0.46
supercoil radius, r_0 (Å)	7.4	8.0	7.5	6.8	7.1	6.9	7.2	7.4
supercoil pitch, P (Å)	187	252	189	213	179	161	191	156
no. of residues per supercoil turn, n	128	171	130	143	119	111	130	107
pairwise helix-crossing angle, Ω (deg)	22	16	23	22	22	23	24	20
pairwise interhelix distance, D (Å)	8.6, 10.0	9.2, 11.0	9.3, 10.8	7.9, 10.5	7.9, 10.9	7.7, 9.3	9.5	9.8

[a] Residues 7−23 of Rop (PDB entry 1ROP) (*84*), 26−51 of WSPLB 21−52 (1YOD) (*85*), 3−31 of E20C (2CCN) (*56*), 341−355 of *lac* repressor (1LBI) (*12*), 3−31 of GCN4-pA (2B1F) (*42*), 5−36 of SARS C44 (1ZV7) (*57*), 5−31 of GCN4-pV (2B22) (*42*), and 5−31 of GCN4-pAe$_{LV}$ were used in the calculations.

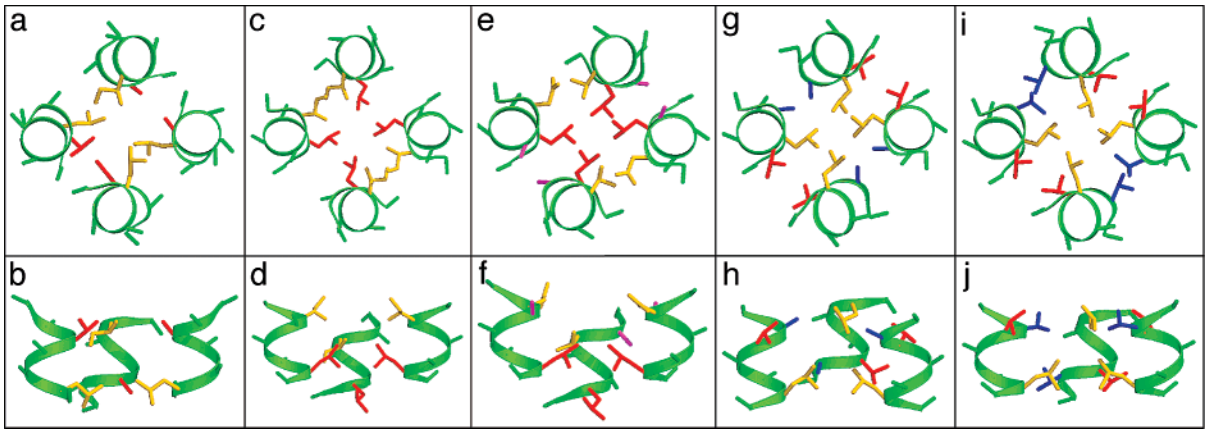

FIGURE 4: Five types of packing interactions in antiparallel four-stranded coiled coils. (a) Helix cross-sectional layers centered on the *a* and *d* positions with a vertical offset of a full turn (0.43 heptad). The backbones of the aligned Rop helices are shown in green C$^{\alpha}$ representation, highlighting core *a* (red) and *d* (yellow) residues. Side chains at positions *b*, *c*, *e*, *f*, and *g* are truncated beyond the C$^{\beta}$ atom for clarity. (b) Side view of the aligned Rop helices. The front helix in the tetramer is omitted to facilitate visualization of the interfacial side chains. (c) Helix cross-sectional layers centered on the *a* and *d* positions with a vertical offset of half a turn (0.28 heptad). The backbones of the shifted E20C helices are shown in green C$^{\alpha}$ representation, highlighting core *a* (red) and *d* (yellow) residues. Side chains at positions *b*, *c*, *e*, *f*, and *g* are truncated beyond the C$^{\beta}$ atom for clarity. (d) Side view of the shifted E20C helices. The front helix in the tetramer is omitted. (e) Helix cross-sectional layers centered on the *a*, *d*, and *e* positions with a vertical offset of half a turn (0.26 heptad). The backbones of the shifted GCN4-pAe$_{LV}$ helices are shown in green C$^{\alpha}$ representation, highlighting core *a* (red), *d* (yellow), and *e* (magenta) residues. Side chains at positions *b*, *c*, *f*, and *g* are truncated beyond the C$^{\beta}$ atom for clarity. (f) Side view of the shifted GCN4-pAe$_{LV}$ helices. The front helix in the tetramer is omitted. (g) Helix cross-sectional layers centered on the *a*, *d*, and *g* positions with a vertical offset of half a turn (0.31 heptad). The backbones of the shifted GCN4-pA helices are shown in green C$^{\alpha}$ representation, highlighting core *a* (red), *d* (yellow), and *g* (blue) residues. Side chains at positions *b*, *c*, *e*, and *f* are truncated beyond the C$^{\beta}$ atom for clarity. (h) Side view of the shifted GCN4-pA helices. The front helix in the tetramer is omitted. (i) Helix cross-sectional layers centered on the *a*, *d*, and *g* positions with a vertical offset of a full turn (0.46 heptad). The backbones of the aligned GCN4-pV helices are shown in green C$^{\alpha}$ representation, highlighting core *a* (red), *d* (yellow), and *g* (blue) residues. Side chains at positions *b*, *c*, *e*, and *f* are truncated beyond the C$^{\beta}$ atom for clarity. (i) Side view of the aligned GCN4-pV helices. The front helix in the tetramer is omitted.

to the opposing directions of side chains in an antiparallel helical array (*56*). Thus, avoidance of steric clashing between bulky hydrophobic residues at the *a* and *d* positions is likely to provide a bias toward the shifted tetramer configuration. Previous studies have suggested that "steric matching" is an important determinant of helix-orientation specificity in other types of antiparallel coiled coils (*27*−*31*).

GCN4-pAe$_{LV}$ described here exhibits the *lac* repressor type of the shifted, antiparallel tetramer structure (Figure 4e,f), because tight packing between neighboring helices is required to bury alanine residues at the *e* positions, and side chains at the *d* positions point toward the tetramer interface (*44*). When adjacent antiparallel helices are aligned, the layering effect of these buried heptad positions would lead to steric clashes between the C$^{\gamma}$ atoms of the *d* residues and the C$^{\delta}$ atoms of the *a* leucines of the adjacent, clockwise-related monomer. Consequently, GCN4-pAe$_{LV}$ exhibits a characteristic interhelical offset of ∼0.25 heptad as a result of their efficient van der Waals packing with a distance of ∼3.8 Å (Figure 3b). Similarly, the GCN4-pA peptide (with alanine at each *g* position) forms an antiparallel tetramer with a 7.7 Å by 9.3 Å rectanglular cross-section and ∼0.25 heptad offset (Figure 4g,h, Table 2) (*42*). In a pair of closely associating helices, the methyl groups must choose one side of the diamond and pack into a triangle of residues on the antiparallel adjacent helix to optimize van der Waals packing of the hydrophobic core (*44*). Thus, the small alanine side chains direct formation of the shifted, antiparallel tetramer. Consistent with this idea, GCN4-pV (with bulkier valine at each *g* position) folds into an aligned, antiparallel tetramer with the ∼0.5 heptad offset (Figure 4i,j) (*42*). GCN4-pV has a square cross-section with an increased interhelical distance of 9.8 Å that accommodates the larger valine side chains in the hydrophobic core of the aligned tetramer. Evidently, the specific topologies of the antiparallel tetrameric coiled coils are determined by the precise interdigitation of the core side chains.

It is interesting to note that the GCN4-pAe peptide, which differs from GCN4-pAe$_{LV}$ by inversion of the valine and leucine substitutions at the *a* and *d* positions, is incompletely

folded in solution (*66*). This observation suggests that the folding of GCN4-pAe$_{LV}$ is driven primarily by the requirement for the larger leucine residues at the central *a* positions to interact in knobs-against-knobs packing, while the smaller valine residues at the peripheral *d* positions interlock via knobs-into-holes packing. In general, antiparallel *a*−*d*−*e* tetrameric coiled coils tend to place bulky hydrophobic side chains at the *a* and *d* positions, with alanines at the *e* positions. As discussed above, both Alacoil sequence motifs allow close packing and stabilization of interhelical contacts (*11*, *44*, *76*, *77*). GCN4-pAe$_{LV}$ shows a preference for an antiparallel tetramer configuration with 0.25 heptad offset. In GCN4-pV, the occurrence of bulky hydrophobic residues at the central *d* positions, with smaller nonpolar side chains of similar size at both peripheral *a* and *g* positions, favors fully aligned, antiparallel tetramers (Table 2). In contrast, GCN4-pA, with alanines at the *g* positions, adopts a shifted, antiparallel tetramer conformation (Table 2).

Specific van der Waals interactions of the core *a* and *d* residues have been shown to determine the stoichiometry and geometry of parallel coiled coils (*26*). The rules and mechanisms that govern helix−helix association in antiparallel coiled coils remain incompletely understood. Introduction of nonpolar side chains at the *e* and/or *g* positions notably increases the repertoire of coiled-coil structures (*42*, *56*, *78*, *82*). In particular a variety of extremely stable antiparallel four-helix coiled coils are possible (*42*, *56*). Antiparallel coiled-coil tetramers can adopt different configurations depending on specific packing interactions at the hydrophobic interface (see Figure 1a). While helices in parallel coiled coils are aligned in perfect register, in antiparallel tetramers the helix offset becomes a major structural parameter. Reproduction of the *lac* repressor coiled-coil tetramer structure in the GCN4 leucine-zipper model reveals a subtle interplay between helix register and the compatibility of the shape of the core amino acids with the packing space. In the *lac* repressor, tetramerization of the protein greatly amplifies operator binding. Extension of the coiled-coil tetramerization domain beyond the natural length can in fact further increase repressor activity (*83*). Thus, elucidation of principles governing the structural selectivity within the extended hydrophobic cores can be used to modulate biologically important conformational switches in general.

ACKNOWLEDGMENT

We thank John Schwanof at the National Synchrotron Light Source for support at beamline X4A.

REFERENCES

1. Lewis, M. (2005) The lac repressor, *C. R. Biol. 328*, 521−548.
2. Kercher, M. A., Lu, P., and Lewis, M. (1997) Lac repressor-operator complex, *Curr. Opin. Struct. Biol. 7*, 76−85.
3. Alberti, S., Oehler, S., von Wilcken-Bergmann, B., Kramer, H., and Muller-Hill, B. (1991) Dimer-to-tetramer assembly of Lac repressor involves a leucine heptad repeat, *New Biol. 3*, 57−62.
4. Chakerian, A. E., Tesmer, V. M., Manly, S. P., Brackett, J. K., Lynch, M. J., Hoh, J. T., and Matthews, K. S. (1991) Evidence for leucine zipper motif in lactose repressor protein, *J. Biol. Chem. 266*, 1371−1374.
5. Lupas, A. (1997) Predicting coiled-coil regions in proteins, *Curr. Opin. Struct. Biol. 7*, 388−393.
6. Alberti, S., Oehler, S., von Wilcken-Bergmann, B., and Muller-Hill, B. (1993) Genetic analysis of the leucine heptad repeats of Lac repressor: evidence for a 4-helical bundle, *EMBO J. 12*, 3227−3236.
7. Brenowitz, M., Mandal, N., Pickar, A., Jamison, E., and Adhya, S. (1991) DNA-binding properties of a lac repressor mutant incapable of forming tetramers, *J. Biol. Chem. 266*, 1281−1288.
8. Chen, J., and Matthews, K. S. (1992) Deletion of lactose repressor carboxyl-terminal domain affects tetramer formation, *J. Biol. Chem. 267*, 13843−13850.
9. Oehler, S., Eismann, E. R., Kramer, H., and Muller-Hill, B. (1990) The three operators of the lac operon cooperate in repression, *EMBO J. 9*, 973−979.
10. Fairman, R., Chao, H. G., Mueller, L., Lavoie, T. B., Shen, L., Novotny, J., and Matsueda, G. R. (1995) Characterization of a new four-chain coiled-coil: influence of chain length on stability, *Protein Sci. 4*, 1457−1469.
11. Solan, A., Ratia, K., and Fairman, R. (2002) Exploring the role of alanine in the structure of the Lac repressor tetramerization domain, a ferritin-like Alacoil, *J. Mol. Biol. 317*, 601−612.
12. Lewis, M., Chang, G., Horton, N. C., Kercher, M. A., Pace, H. C., Schumacher, M. A., Brennan, R. G., and Lu, P. (1996) Crystal structure of the lactose operon repressor and its complexes with DNA and inducer, *Science (Washington, D.C.) 271*, 1247−1254.
13. Friedman, A. M., Fischmann, T. O., and Steitz, T. A. (1995) Crystal structure of lac repressor core tetramer and its implications for DNA looping, *Science (Washington, D.C.) 268*, 1721−1727.
14. Oakley, M. G., and Hollenbeck, J. J. (2001) The design of antiparallel coiled coils, *Curr. Opin. Struct. Biol. 11*, 450−457.
15. Woolfson, D. N. (2005) The design of coiled-coil structures and assemblies, *Adv. Protein Chem. 70*, 79−112.
16. Lupas, A. N., and Gruber, M. (2005) The structure of alpha-helical coiled coils, *Adv. Protein Chem. 70*, 37−78.
17. Kohn, W. D., Mant, C. T., and Hodges, R. S. (1997) Alpha-helical protein assembly motifs, *J. Biol. Chem. 272*, 2583−2586.
18. Bryson, J. W., Betz, S. F., Lu, H. S., Suich, D. J., Zhou, H. X., O'Neil, K. T., and DeGrado, W. F. (1995) Protein design: a hierarchic approach, *Science (Washington, D.C.) 270*, 935−941.
19. Burkhard, P., Stetefeld, J., and Strelkov, S. V. (2001) Coiled coils: a highly versatile protein folding motif, *Trends Cell Biol. 11*, 82−88.
20. Mason, J. M., and Arndt, K. M. (2004) Coiled coil domains: stability, specificity, and biological implications, *ChemBioChem 5*, 170−176.
21. McLachlan, A. D., and Stewart, M. (1975) Tropomyosin coiled-coil interactions: evidence for an unstaggered structure, *J. Mol. Biol. 98*, 293−304.
22. Parry, D. A. (1982) Coiled-coils in alpha-helix-containing proteins: analysis of the residue types within the heptad repeat and the use of these data in the prediction of coiled-coils in other proteins, *Biosci. Rep. 2*, 1017−1024.
23. Lupas, A., Van Dyke, M., and Stock, J. (1991) Predicting coiled coils from protein sequences, *Science (Washington, D.C.) 252*, 1162−1164.
24. Hodges, R. S., Sodek, J., Smillie, L. B., and Jurasek, L. (1972) Tropomyosin: Amino acid sequence and coiled-coil structure, *Cold Spring Harbor Symp. Quant. Biol. 37*, 299−310.
25. Crick, F. H. C. (1953) The packing of α-helices: simple coiled-coils, *Acta Crystallogr. 6*, 689−697.
26. Harbury, P. B., Zhang, T., Kim, P. S., and Alber, T. (1993) A switch between two-, three-, and four-stranded coiled coils in GCN4 leucine zipper mutants, *Science (Washington, D.C.) 262*, 1401−1407.
27. Gurnon, D. G., Whitaker, J. A., and Oakley, M. G. (2003) Design and characterization of a homodimeric antiparallel coiled coil, *J. Am. Chem. Soc. 125*, 7518−7519.
28. Monera, O. D., Zhou, N. E., Lavigne, P., Kay, C. M., and Hodges, R. S. (1996) Formation of parallel and antiparallel coiled-coils controlled by the relative positions of alanine residues in the hydrophobic core, *J. Biol. Chem. 271*, 3995−4001.
29. Betz, S. F., and DeGrado, W. F. (1996) Controlling topology and native-like behavior of de novo-designed peptides: design and characterization of antiparallel four-stranded coiled coils, *Biochemistry 35*, 6955−6962.
30. Schnarr, N. A., and Kennan, A. J. (2004) Strand orientation by steric matching: a designed antiparallel coiled-coil trimer, *J. Am. Chem. Soc. 126*, 14447−14451.

31. Munson, M., O'Brien, R., Sturtevant, J. M., and Regan, L. (1994) Redesigning the hydrophobic core of a four-helix-bundle protein, *Protein Sci. 3*, 2015−2022.
32. Lumb, K. J., and Kim, P. S. (1995) A buried polar interaction imparts structural uniqueness in a designed heterodimeric coiled coil, *Biochemistry 34*, 8642−8648.
33. Gonzalez, L., Jr., Woolfson, D. N., and Alber, T. (1996) Buried polar residues and structural specificity in the GCN4 leucine zipper, *Nat. Struct. Biol. 3*, 1011−1018.
34. Betz, S. F., Bryson, J. W., and DeGrado, W. F. (1995) Native-like and structurally characterized designed alpha-helical bundles, *Curr. Opin. Struct. Biol. 5*, 457−463.
35. Oakley, M. G., and Kim, P. S. (1998) A buried polar interaction can direct the relative orientation of helices in a coiled coil, *Biochemistry 37*, 12603−12610.
36. O'Shea, E. K., Lumb, K. J., and Kim, P. S. (1993) Peptide 'Velcro': Design of a heterodimeric coiled coil, *Curr. Biol. 3*, 658−667.
37. Krylov, D., Mikhailenko, I., and Vinson, C. (1994) A thermodynamic scale for leucine zipper stability and dimerization specificity: e and g interhelical interactions, *EMBO J. 13*, 2849−2861.
38. Monera, O. D., Kay, C. M., and Hodges, R. S. (1994) Electrostatic interactions control the parallel and antiparallel orientation of alpha-helical chains in two-stranded alpha-helical coiled-coils, *Biochemistry 33*, 3862−3871.
39. Zeng, X., Zhu, H., Lashuel, H. A., and Hu, J. C. (1997) Oligomerization properties of GCN4 leucine zipper e and g position mutants, *Protein Sci. 6*, 2218−2226.
40. Kohn, W. D., Kay, C. M., and Hodges, R. S. (1998) Orientation, positional, additivity, and oligomerization-state effects of interhelical ion pairs in alpha-helical coiled-coils, *J. Mol. Biol. 283*, 993−1012.
41. McClain, D. L., Binfet, J. P., and Oakley, M. G. (2001) Evaluation of the energetic contribution of interhelical Coulombic interactions for coiled coil helix orientation specificity, *J. Mol. Biol. 313*, 371−383.
42. Deng, Y., Liu, J., Zheng, Q., Eliezer, D., Kallenbach, N. R., and Lu, M. (2006) Antiparallel four-stranded coiled coil specified by a 3-3-1 hydrophobic heptad repeat, *Structure 14*, 247−255.
43. Monera, O. D., Zhou, N. E., Kay, C. M., and Hodges, R. S. (1993) Comparison of antiparallel and parallel two-stranded alpha-helical coiled-coils. Design, synthesis, and characterization, *J. Biol. Chem. 268*, 19218−19227.
44. Gernert, K. M., Surles, M. C., Labean, T. H., Richardson, J. S., and Richardson, D. C. (1995) The Alacoil: a very tight, antiparallel coiled-coil of helices, *Protein Sci. 4*, 2252−2260.
45. Berger, B., Wilson, D. B., Wolf, E., Tonchev, T., Milla, M., and Kim, P. S. (1995) Predicting coiled coils by use of pairwise residue correlations, *Proc. Natl. Acad. Sci. U.S.A. 92*, 8259−8263.
46. Conway, J. F., and Parry, D. A. (1991) Three-stranded alpha-fibrous proteins: the heptad repeat and its implications for structure, *Int. J. Biol. Macromol. 13*, 14−16.
47. Conway, J. F., and Parry, D. A. (1990) Structural features in the heptad substructure and longer range repeats of two-stranded alpha-fibrous proteins, *Int. J. Biol. Macromol. 12*, 328−334.
48. Walshaw, J., and Woolfson, D. N. (2001) Socket: a program for identifying and analysing coiled-coil motifs within protein structures, *J. Mol. Biol. 307*, 1427−1450.
49. Woolfson, D. N., and Alber, T. (1995) Predicting oligomerization states of coiled coils, *Protein Sci. 4*, 1596−1607.
50. Wolf, E., Kim, P. S., and Berger, B. (1997) MultiCoil: a program for predicting two- and three-stranded coiled coils, *Protein Sci. 6*, 1179−1189.
51. Fong, J. H., Keating, A. E., and Singh, M. (2004) Predicting specificity in bZIP coiled-coil protein interactions, *Genome Biol. 5*, R11.
52. Havranek, J. J., and Harbury, P. B. (2003) Automated design of specificity in molecular recognition, *Nat. Struct. Biol. 10*, 45−52.
53. Grigoryan, G., and Keating, A. E. (2006) Structure-based prediction of bZIP partnering specificity, *J. Mol. Biol. 355*, 1125−1142.
54. McClain, D. L., Woods, H. L., and Oakley, M. G. (2001) Design and characterization of a heterodimeric coiled coil that forms exclusively with an antiparallel relative helix orientation, *J. Am. Chem. Soc. 123*, 3151−3152.
55. Ghosh, I., Hamilton, A. D., and Regan, L. (2000) Antiparallel leucine zipper-directed protein reassembly: application to the green fluorescent protein, *J. Am. Chem. Soc. 122*, 5658−5659.
56. Yadav, M. K., Leman, L. J., Price, D. J., Brooks, Iii, C. L., Stout, C. D., and Ghadiri, M. R. (2006) Coiled coils at the edge of configurational heterogeneity. Structural analyses of parallel and antiparallel homotetrameric coiled coils reveal configurational sensitivity to a single solvent-exposed amino Acid substitution, *Biochemistry 45*, 4463−4473.
57. Deng, Y., Liu, J., Zheng, Q., Yong, W., and Lu, M. (2006) Structures and polymorphic interactions of two heptad-repeat regions of the SARS virus S2 protein, *Structure 14*, 889−899.
58. Edelhoch, H. (1967) Spectroscopic determination of tryptophan and tyrosine in proteins, *Biochemistry 6*, 1948−1954.
59. Chen, Y. H., Yang, J. T., and Chau, K. H. (1974) Determination of the helix and beta form of proteins in aqueous solution by circular dichroism, *Biochemistry 13*, 3350−3359.
60. Cantor, C., and Schimmel, P. (1980) *Biophysical Chemistry*, Vol. III, W. H. Freeman and Co., New York.
61. Shu, W., Ji, H., and Lu, M. (1999) Trimerization specificity in HIV-1 gp41: analysis with a GCN4 leucine zipper model, *Biochemistry 38*, 5378−5385.
62. Johnson, M. L., Correia, J. J., Yphantis, D. A., and Halvorson, H. R. (1981) Analysis of data from the analytical ultracentrifuge by nonlinear least-squares techniques, *Biophys. J. 36*, 575−588.
63. Laue, T. M., Shah, B. D., Ridgeway, T. M., and Pelletier, S. L. (1992) Computer-aided interpretation of analytical sedimentation data for proteins, in *Analytical Ultracentrifugation in Biochemistry and Polymer Science* (Harding, S. E., Rowe, A. J., and Horton, J. C., Eds.) pp 90−125, Royal Society of Chemistry, Cambridge, U.K.
64. Otwinowski, Z., and Minor, W. (1997) Processing X-ray diffraction data collected in oscillation mode, *Methods Enzymol. 276*, 307−326.
65. Storoni, L. C., McCoy, A. J., and Read, R. J. (2004) Likelihood-enhanced fast rotation functions, *Acta Crystallogr., D: Biol. Crystallogr. 60*, 432−438.
66. Deng, Y., Zheng, Q., Liu, J., Cheng, C. S., Kallenbach, N. R., and Lu, M. (2007) Self-assembly of coiled-coil tetramers in the 1.40 A structure of a leucine-zipper mutant, *Protein Sci. 16*, 323−328.
67. Lamzin, V. S., and Wilson, K. S. (1993) Automated refinement of protein models, *Acta Crystallogr., D: Biol. Crystallogr. 49*, 129−149.
68. Murshudov, G. N., Vagin, A. A., and Dodson, E. J. (1997) Refinement of macromolecular structures by the maximum-likehood method, *Acta Crystallogr., D: Biol. Crystallogr. 53*, 240−255.
69. Jones, T. A., Zou, J. Y., Cowan, S. W., and Kjeldgaard. (1991) Improved methods for building protein models in electron density maps and the location of errors in these models, *Acta Crystallogr., A: Found. Crystallogr. 47* (Part 2), 110−119.
70. Strelkov, S. V., and Burkhard, P. (2002) Analysis of alpha-helical coiled coils with the program TWISTER reveals a structural mechanism for stutter compensation, *J. Struct. Biol. 137*, 54−64.
71. Potterton, E., Briggs, P., Turkenburg, M., and Dodson, E. (2003) A graphical user interface to the CCP4 program suite, *Acta Crystallogr., D: Biol. Crystallogr. 59*, 1131−1137.
72. Brunger, A. T., Adams, P. D., Clore, G. M., DeLano, W. L., Gros, P., Grosse-Kunstleve, R. W., Jiang, J. S., Kuszewski, J., Nilges, M., Pannu, N. S., Read, R. J., Rice, L. M., Simonson, T., and Warren, G. L. (1998) Crystallography & NMR system: A new software suite for macromolecular structure determination, *Acta Crystallogr., D: Biol. Crystallogr. 54* (Part 5), 905−921.
73. Evans, S. V. (1993) SETOR: hardware-lighted three-dimensional solid model representations of macromolecules, *J. Mol. Graphics 11*, 134−138.
74. Kraulis, P. J. (1991) A program to produce both detailed and schematic plots of protein structures, *J. Appl. Crystallogr. 24*, 946−950.
75. Merritt, E. A., and Bacon, D. J. (1997) Raster 3D: photorealistic molecular graphics, *Methods Enzymol. 277*, 505−524.
76. Ogihara, N. L., Ghirlanda, G., Bryson, J. W., Gingery, M., DeGrado, W. F., and Eisenberg, D. (2001) Design of three-dimensional domain-swapped dimers and fibrous oligomers, *Proc. Natl. Acad. Sci. U.S.A. 98*, 1404−1409.
77. North, B., Summa, C. M., Ghirlanda, G., and DeGrado, W. F. (2001) D(n)-symmetrical tertiary templates for the design of tubular proteins, *J. Mol. Biol. 311*, 1081−1090.
78. Liu, J., Deng, Y., Zheng, Q., Cheng, C. S., Kallenbach, N. R., and Lu, M. (2006) A parallel coiled-coil tetramer with offset helices, *Biochemistry 45*, 15224−15231.

79. O'Shea, E. K., Klemm, J. D., Kim, P. S., and Alber, T. (1991) X-ray structure of the GCN4 leucine zipper, a two-stranded, parallel coiled coil, *Science (Washington, D.C.) 254*, 539−544.
80. Lovell, S. C., Word, J. M., Richardson, J. S., and Richardson, D. C. (2000) The penultimate rotamer library, *Proteins 40*, 389−408.
81. Schafmeister, C. E., Miercke, L. J., and Stroud, R. M. (1993) Structure at 2.5 A of a designed peptide that maintains solubility of membrane proteins, *Science (Washington, D.C.) 262*, 734−738.
82. Liu, J., Zheng, Q., Deng, Y., Cheng, C. S., Kallenbach, N. R., and Lu, M. (2006) A seven-helix coiled coil, *Proc. Natl. Acad. Sci. U.S.A. 103*, 15457−15462.
83. Fieck, A., Wyborski, D. L., and Short, J. M. (1992) Modifications of the E. coli Lac repressor for expression in eukaryotic cells: effects of nuclear signal sequences on protein activity and nuclear accumulation, *Nucleic Acids Res. 20*, 1785−1791.
84. Banner, D. W., Cesareni, G., and Tsernoglou, D. (1983) Crystallization of the ColE1 Rop protein, *J. Mol. Biol. 170*, 1059−1060.
85. Slovic, A. M., Stayrook, S. E., North, B., and Degrado, W. F. (2005) X-ray structure of a water-soluble analog of the membrane protein phospholamban: sequence determinants defining the topology of tetrameric and pentameric coiled coils, *J. Mol. Biol. 348*, 777−787.

BI701930D